3D topology optimization of a tall tower considering soil flexibility

Iago Cavalcante[1], Renato Picelli[2], Josué Labaki[1]

[1]*School of Mechanical Engineering, University of Campinas - Unicamp*
200 Mendeleyev St, 13083-970, Campinas SP Brazil
i209496@dac.unicamp.br, labaki@unicamp.br
[2]*Polytechnic School, University of São Paulo - USP*
Col. Narciso de Andrade Square, 11013-552, Santos SP Brazil
rpicelli@usp.br

Abstract. This paper investigates the effect of soil flexibility on the solution obtained by topology optimization of a tall tower in continuous contact with the soil throughout its base. The tower is modeled with classical finite elements, while the soil is modeled with boundary elements, which is more adequate to deal with unbounded soil domains. Coupling between the tower and soil is established by imposing equilibrium and continuity conditions at the soil–tower interface. The paper shows strategies for solving the different orders and types of elements at that interface. The final equilibrium equation resulting from the coupling scheme contains the linear superposition of the tower and soil stiffness matrices, and connects nodal forces and displacements as in classical finite element assembly schemes. The Bi-Directional Evolutionary Structural Optimization method (BESO) is chosen to solve the compliance minimization problem under prescribed volume constraints. The solutions for the tower resting on the ground surface and for resting on rigid supports are compared, and the results show that both the optimal topology of the tower and the compliance that is achievable are significantly affected by the flexibility of the soil.

Keywords: Topology optimization, Coupled methods, Soil-structure interaction.

1 Introduction

The past few decades have witnessed the rise of a wide variety of topology optimization methods. The Solid Isotropic Material with Penalization (SIMP) [1], the Level Set Topology Optimization (LSTO) [2], the Uni-directional Evolutionary Structural Optimization (ESO) [3] and its Bi-directional counterpart (BESO) [4], and the Topology Optimization of Binary Structures (TOBS) [5] methods are a few examples of improvements on Bendsøe and Kikuchi [6]'s original propositions. Applications have been explored in a wide range of problems, from elementary elasticity [7] to multiphysics [8] and multiscale [9] problems. These, however, are strongly focused on bounded-domain problems, which is understandable considering the practical interest in such problems.

A class of unbounded-domain problems of relevant practical interest is soil-structure interaction problems. The flexibility of the soil and foundation has significant impact in the response of the structure they support [10], and the literature has been sparse with regards to their effect in the topology optimization solution. The most noteworthy results in this regard are the ESO and BESO studies of 2D and 3D excavations presented by Ren et al. [11], Ren et al. [12], Eliáš et al. [13] and Sobótka [14]. Seitz and Grabe [15] considered optimization of buried foundations on granular soils. However, the only known result to consider the effect of soil and foundation flexibility in the topology optimization of the structure is that by Cavalcante et al. [16], which showed that the presence of the foundation has a significant effect in both the final topology of the structure and in the achievable optimization result. Their study, however, is limited by considering the foundation as one-dimensional piles interacting with the structure at discrete points. The effect of continuous contact with the soil, which is common in engineering practice and should have a more significant effect in the topology optimization of the structure, is yet to be considered in the literature.

In this paper, we consider the problem of topology optimization of a structure in continuous contact with the soil. The representative problem of a tall tower is selected for this analysis. The tower is modeled with

classical finite elements, while the soil is modeled with boundary elements, which is more adequate to deal with unbounded domains such as the soil. Coupling between the tower and soil is established by imposing equilibrium and continuity conditions at the soil–tower interface. This process requires careful consideration of the different orders and types of elements at that interface. The resulting equilibrium equation is written in terms of nodal displacements and forces of the tower, and incorporates the effect of the flexibility of the soil in its stiffness matrix. This equilibrium equation then undergoes topology optimization through classical BESO.

1.1 Problem statement

Consider a tower with initial optimization domain of sides $5a \times 5a$ and height $15a$, Young's modulus E_t and Poisson ratio ν_t. Centered at the top surface of the tower, a square $a \times a$ patch is under uniformly distributed horizontal ($y-$direction) and vertical ($z-$direction) loads. The loaded patch is a non-design domain: it is prescribed not to be affected by the optimization procedure. The tower is in perfectly bonded contact with a homogeneous, isotropic half-space with Young's modulus E and Poisson ratio ν. The objective function is to minimize the compliance of the tower under a prescribed target volume reduction. BESO is used to analyze the difference between the optimized topologies for the cases in which the tower rests on the surface of the soil and the case in which it rests over rigid supports.

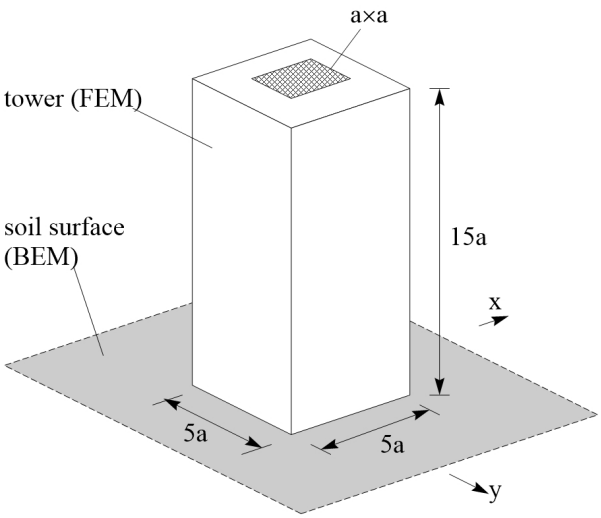

Figure 1. Tower interacting with the soil.

2 Numerical models

2.1 Model of the structure

In this paper, the tower is modeled with classical linear-elastic 8-noded hexahedral finite elements with three degrees of freedom per node. Nodal displacements and forces in the finite element mesh of the discretized tower are related through

$$\boldsymbol{F_t} = \boldsymbol{K_t U_t} \tag{1}$$

in which $\boldsymbol{F_t}$ and $\boldsymbol{U_t}$ are the vector of nodal forces and nodal displacements, and $\boldsymbol{K_t}$ is the global stiffness matrix of the tower. Global $\boldsymbol{K_t}$ is assembled from the elemental stiffness matrices [17], given by

$$\boldsymbol{k_e} = \int_{V_e} \boldsymbol{B}^T \boldsymbol{D} \boldsymbol{B} dV_e = \int_{-1}^{1}\int_{-1}^{1}\int_{-1}^{1} \boldsymbol{B}^T \boldsymbol{D} \boldsymbol{B} \det(J)\, d\xi d\eta d\zeta, \tag{2}$$

in which V_e is the volume of the element, $\boldsymbol{D}$ is the constitutive matrix of the element, $\boldsymbol{N}$ is the matrix of linear shape functions, $\boldsymbol{B}$ is the matrix of derivatives of the terms of $\boldsymbol{N}$, and J is the Jacobian that relates the formulations of the element in the physical and natural domains. For a full description of the terms involved in eq. 2, refer to Bathe [17].

2.2 Soil model

A boundary element framework is used to model the soil in this analysis. This framework resorts to superposition of non-singular Green's functions (influence functions) to obtain the displacement fields at the tower–soil interface. The surface of the soil is discretized into M boundary elements, which is the same number of finite elements of the mesh of the tower in the tower–soil interface. Considering the hexahedral elements used to discretize the tower, rectangular boundary elements are used in this case. Each element l is defined within the bounds of $-A \leq x \leq A$ and $-B \leq y \leq B$ at the surface of the half-space ($z = 0$), centered at (x_l, y_l). The surface traction and displacement vectors of the half-space due to normal p_z and in-plane loads p_x and p_y are, respectively, $\boldsymbol{t} = p_x \mathrm{e}_x + p_y \mathrm{e}_y + p_z \mathrm{e}_z$ and $\boldsymbol{u} = u_x \mathrm{e}_x + u_y \mathrm{e}_y + u_z \mathrm{e}_z$. The effect of $\boldsymbol{t}$ over the M elements is measured at arbitrary elements k, centered at $(x_k, y_k, z = 0)$. Assuming constant traction distribution over the elements, Willner [18] derived solutions for the displacement influence functions for the half-space. These solutions are based on direct analytical integration of the Boussinesq [19] and Cerruti [20] solutions for point loads over the area of the element. The fully-coupled displacement–traction relation is

$$u_{xk} = \sum_{l=1}^{M} \left(c_{kl}^{xx} p_{xl} + c_{kl}^{xy} p_{yl} + c_{kl}^{xz} p_{zl} \right) \tag{3}$$

$$u_{yk} = \sum_{l=1}^{M} \left(c_{kl}^{yx} p_{xl} + c_{kl}^{yy} p_{yl} + c_{kl}^{yz} p_{zl} \right) \tag{4}$$

$$u_{zk} = \sum_{l=1}^{M} \left(c_{kl}^{zx} p_{xl} + c_{kl}^{zy} p_{yl} + c_{kl}^{zz} p_{zl} \right) \tag{5}$$

in which, for example,

$$c_{kl}^{xx} = \frac{1}{2\pi G} \int_{-A}^{A} \int_{-B}^{B} \left\{ \frac{1-\nu}{\rho_{kl}} + \frac{\nu \left(x_k - x_l - \xi \right)^2}{\rho_{kl}^3} \right\} d\eta \, d\xi, \tag{6}$$

in which $G = 1/2E/(1+\nu)$ is the shear modulus of the half-space, and $\rho_{kl} = \sqrt{\left(x_k - x_l - \xi \right)^2 + \left(y_k - y_l - \eta \right)^2}$. Willner [18] obtained closed-form expressions for these influence terms. In the case of c_{kl}^{xx}, these are

$$c_{kl}^{xx} = \frac{1}{2\pi G} \left\{ (1-\nu)(x+A) \ln(G_1) + (1-\nu)(x-A) \ln(G_2) + (y+B) \ln(G_3) + (y-B) \ln(G_4) \right\},$$

in which

$$G_1 = \frac{y + B + \sqrt{(x+A)^2 + (y+B)^2}}{y - B + \sqrt{(x+A)^2 + (y-B)^2}},$$

$$G_2 = \frac{y - B + \sqrt{(x-A)^2 + (y-B)^2}}{y + B + \sqrt{(x-A)^2 + (y+B)^2}},$$

$$G_3 = \frac{x + A + \sqrt{(x+A)^2 + (y+B)^2}}{x - A + \sqrt{(x-A)^2 + (y+B)^2}},$$

$$G_4 = \frac{x - A + \sqrt{(x-A)^2 + (y-B)^2}}{x + A + \sqrt{(x+A)^2 + (y-B)^2}}.$$

The expressions for the remaining influence terms c_{kl}^{rs} ($r, s = x, y, z$) in eqs. 3 to 5 can be found in [18]. For future reference, eqs. 3 to 5 can be organized in matrix form as

$$\boldsymbol{u} = \boldsymbol{U} \boldsymbol{t}, \tag{7}$$

in which $\boldsymbol{U}$ is referred to as the soil influence matrix, each term of which contains c_{kl}^{rs}.

2.3 Coupling scheme

In this analysis, the tower is assumed to be in fully-bonded contact with the surface of the soil. Coupling under this condition is obtained by imposing continuity and equilibrium conditions at the tower–half-space interface. Considering that the tower and the half-space are discretized with elements of different types and orders, a careful consideration of these differences is necessary while establishing the coupling.

The equilibrium equation for the nodes at the tower–half-space interface is a modification from eq. 1, with the inclusion of $\boldsymbol{F_s}$ representing the vector of equivalent nodal contact forces due to the presence of the half-space [21]:

$$\boldsymbol{F_t} = \boldsymbol{K_t U_t} + \boldsymbol{F_s}. \tag{8}$$

The distribution of the contact traction $\boldsymbol{F_s}$ is unknown. It can be approximated by piece-wise constant tractions $\boldsymbol{t}$, which are the tractions acting at the boundary elements of the half-space. $\boldsymbol{F_s}$ and $\boldsymbol{t}$ are related through

$$\boldsymbol{F_s} = \boldsymbol{A t}, \tag{9}$$

in which the transformation matrix $\boldsymbol{A}$ is responsible for mapping constant tractions $\boldsymbol{t}$ in each boundary element into their nodal equivalent $\boldsymbol{F_s}$ in each finite element. The equilibrium equation then becomes

$$\boldsymbol{F_t} = \boldsymbol{K_t U_t} + \boldsymbol{A t}. \tag{10}$$

Similarly, boundary element displacements (eqs. 3 to 5), which are measured at the center of each element, have incompatible dimensions with respect to the four nodes of the finite element of the mesh of the tower. The compatibilization is obtained through the transformation matrix $\boldsymbol{D}$, such that

$$\boldsymbol{u} = \boldsymbol{D U_t}. \tag{11}$$

In view of eq. 11, the continuity condition at the tower–half-space interface yields

$$\boldsymbol{D U_t} = \boldsymbol{U t}, \tag{12}$$

in which $\boldsymbol{U}$ is the influence matrix of the half-space (eq. 7). Equation 12 results from assuming the perfectly bonded condition at the tower–half-space interface. Expressions for $\boldsymbol{A}$ and $\boldsymbol{D}$ can be directly extended from the 2D case presented by Carneiro et al. [21]. Equations 10 and 12 make up the equilibrium equation for the tower–soil system:

$$\begin{bmatrix} \boldsymbol{K_t} & \boldsymbol{A} \\ \boldsymbol{D} & -\boldsymbol{U} \end{bmatrix} \begin{Bmatrix} \boldsymbol{U_t} \\ \boldsymbol{t} \end{Bmatrix} = \begin{Bmatrix} \boldsymbol{F_t} \\ \boldsymbol{0} \end{Bmatrix}. \tag{13}$$

2.4 Optimization method

This paper uses the classical BESO method proposed by Huang and Xie [4]. The method is used here to minimize the compliance $C = \frac{1}{2}\boldsymbol{F_t}^T\boldsymbol{U_t}$ of the system, subjected to $V^f - \sum_{i=1}^{N_e} V_i x_i = 0$, in which V_i is the volume of each of the N_e elements, and V^f is the specified final volume of the structure.

At iteration $k = 1$, the initial design domain of the tower is that of Fig. 1. All elements of this initial domain receive a design variable value $x_i = 1$. Equation 13 is solved, which includes the flexibility of soil. Element sensitivity

$$\alpha_i = \frac{\sum_{j=1}^{N_s} w\left(r_{ij}\right) \alpha_j^n}{\sum_{j=1}^{N_s} w\left(r_{ij}\right)} \tag{14}$$

is computed for all elements, in which N_s is the number of nodes inside an arbitrarily-defined spherical domain Ω of radius r_{min} centered at the center of element i, r_{ij} is the distance between node j and the center of Ω, $w\left(r_{ij}\right) = r_{min} - r_{ij}$ $(j = 1 : N_s)$ is a weight factor, and

$$\alpha_j^n = \frac{\sum_{j=1}^{N_j} V_i \alpha_i^e}{\sum_{j=1}^{N_j} V_i}, \tag{15}$$

in which N_j is the number of elements in connection to j, and $\alpha_i^e = \Delta C_i = \frac{1}{2}\boldsymbol{u_e}_i^T \boldsymbol{k_e} \boldsymbol{u_e}_i$ is the sensitivity related to each element. Huang and Xie [4] proposed yet another sensitivity parameter, $\bar{\alpha}_i = \frac{1}{2}\left(\alpha_i^k - \alpha_i^{k-1}\right)$, which is controlled for all elements above $k = 2$. The change in the volume of the tower between iterations is measured by

$$V_{k+1} = V_k \left(1 \pm \rho\right) \tag{16}$$

in which ρ is the amount by which the volume is prescribed to change. Design variables x_i are switched to 0 or 1 towards achieving V_{k+1}, depending on whether a prescribed sensitivity threshold is met by the element. This iterative scheme is repeated until V^f is achieved, provided that

$$\frac{\sum_{m=1}^{M} C_{k-1+m} - \sum_{m=1}^{M} C_{k-M-m+1}}{\sum_{m=1}^{M} C_{k-m+1}} \leq \tau \tag{17}$$

is met as well, in which M is a given arbitrary integer, and τ is a small tolerance.

3 Numerical results

The present implementation has been thoroughly validated with limiting cases from the literature.

The optimization results in this section consider separately the cases in which the tower is under horizontal ($y-$direction) and vertical ($z-$direction) loads. The tower was discretized into 625 elements in each cross section ($x-y$ plane) by 20 divisions along its height ($z-$direction), resulting in a mesh with 12,500 elements. Consequently, 625 boundary elements were used to discretize the tower–half-space interface. The material properties were selected so that $E_t = 10E$ and $\nu_t = \nu$, which are reasonable values in engineering practice. The optimization procedure considered $\rho = 0.05$, $r_{min} = 1.2a$, $\tau = 10^{-3}$, and $V^f = 0.25V$, in which V is the initial volume of the tower. Figure 2a shows the final optimized topology obtained for the case of tower under horizontal load. The case of tower over rigid supports is shown for comparison in Fig. 2b. This is obtained by classical topology optimization of the finite element mesh of the tower under imposed zero-displacement boundary conditions at the base. The corresponding results for the tower under vertical loads is shown in Figs. 2c and 2d, for the case in which it is supported by the soil and by rigid supports, respectively. Figure 3 shows the evolution of the compliance objective function through the iterations of the optimization algorithm for both cases. These results are presented in terms of the normalized compliance $C_k^* = C_k/C_{k=1}$, which normalizes the compliance of a given iteration k by that of the first iteration ($k = 1$), and of the normalized volume $V_k^* = V_k/V_{k=1}$.

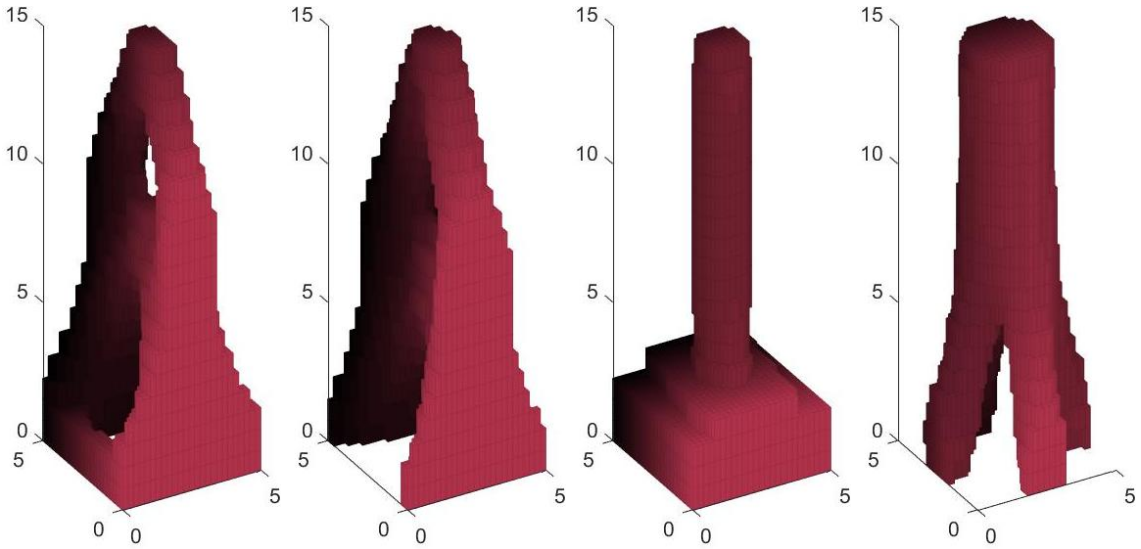

Figure 2. Optimized topology for the tower under horizontal loads (a-b) and vertical loads (c-d). Figures (a) and (c) consider soil support, while Figs. (b) and (d) consider rigid supports.

Figure 2 shows that the presence of the soil has a significant influence in the topology that is obtained by the optimization algorithm. A feature that stands out in the comparison between soil and rigid support cases is that the algorithm resorts to allocating more volume near the base of the tower in the soil support case than in the rigid support case. This is due to the increased flexibility of that portion of the tower due to the presence of the soil, which compromises the overall compliance of the tower in both loading cases. Figure 3a, on the other hand, shows that the effect of the soil flexibility in the compliance that is achievable by the optimization algorithm is negligible in the horizontal loading case. This shows that the optimization algorithm manages to find comparable minima for either support case, which is achieved by the allocation of material in the more flexible parts of the structure. This is not observed in the vertical case (Fig. 3b). In that case, both the optimized topology and the achievable minimal compliance are starkly different between the rigid and soil support cases.

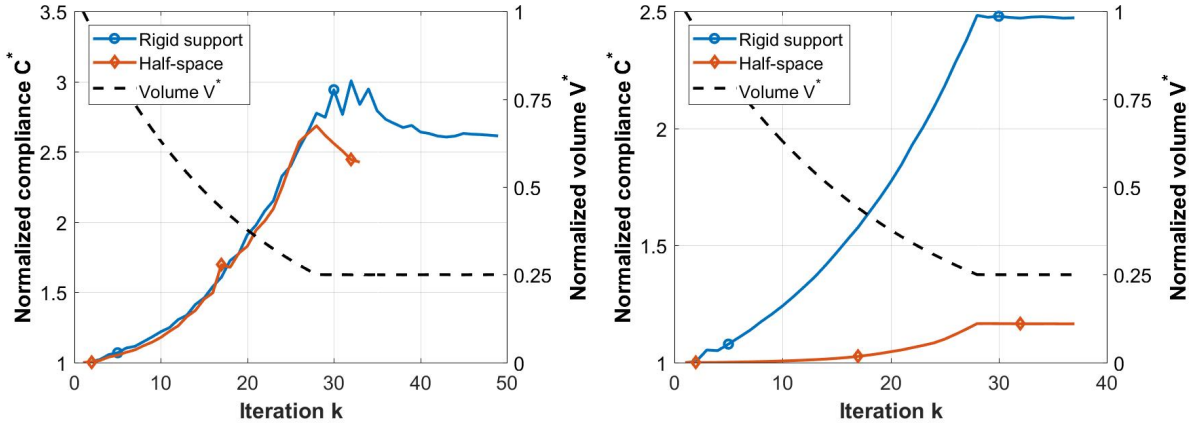

Figure 3. Evolution of the compliance objective function through iterations for the tower under a) horizontal and b) vertical loads.

4 Conclusions

This paper presented a study on the influence of soil flexibility in the topology optimization of a tall tower in continuous contact with the soil. The tower and the soil were modeled via finite and boundary element schemes, respectively. A strategy to deal with the different types and orders of elements at the tower–soil interface was presented. Topology optimization was performed with BESO. The results showed that both the optimized topology and the achievable optimization result may be strongly dependent on whether or not soil flexibility is taken into consideration. This study indicates that it may not be a reasonable assumption to disregard the flexibility of the soil in topology optimization analyses involving soil-structure interaction.

Authorship statement. The authors hereby confirm that they are the sole liable persons responsible for the authorship of this work, and that all material that has been herein included as part of the present paper is either the property (and authorship) of the authors, or has the permission of the owners to be included here.

References

[1] M. P. Bendsoe. "Optimal shape design as a material distribution problem". *Structural Optimization*, vol. 1, pp. 193–202, 1989.
[2] M. Y. Wang, X. Wang, and D. Guo. "A level set method for structural topology optimization". *Computer Methods in Applied Mechanics and Engineering*, vol. 192, n. 1-2, pp. 227–246, 2003.
[3] Q. Xia, T. Shi, S. Liu, and M. Y. Wang. "Optimization of stresses s in a local region for the maximization of sensitivity and minimization of cross - sensitivity of piezoresistive sensors". *Structural and Multidisciplinary Optimization*, vol. 48, pp. 927–938, 2013.
[4] X. Huang and Y. M. Xie. "Convergent and mesh-independent solutions for the bi-directional evolutionary structural optimization method". *Finite Elements in Analysis and Design*, vol. 43, pp. 1039–1049, 2007.
[5] R. Sivapuram and R. Picelli. "Topology optimization of binary structures using integer linear programming". *Finite Elements in Analysis and Design*, vol. 139, pp. 49–61, 2018.
[6] M. P. Bendsøe and N. Kikuchi. "Generating optimal topologies in structural design using a homogenization method". *Computer Methods in Applied Mechanics and Engineering*, vol. 71, pp. 197–224, 1988.
[7] C. Le, J. Norato, T. Bruns, C. Ha, and D. Tortorelli. "Stress-based topology optimization for continua". *Structural and Multidisciplinary Optimization*, vol. 41, pp. 605–620, 2010.
[8] C. Lundgaard, J. Alexandersen, M. Zhou, C. Andreasen, and O. Sigmund. "Revisiting density-based topology optimization for fluid-structure-interaction problems". *Structural and Multidisciplinary Optimization*, vol. 58, n. 3, pp. 969–995, 2018.
[9] Z. Du, X. Y. Zhou, R. Picelli, and H. A. Kim. "Connecting microstructures for multiscale topology optimization with connectivity index constraints". *Journal of Mechanical Design*, vol. 140, n. 11, pp. 111417, 2018.
[10] M. Lou, H. Wang, X. Chen, and Y. Zhai. "Structure–soil–structure interaction: Literature review". *Soil dynamics and earthquake engineering*, vol. 31, n. 12, pp. 1724–1731, 2011.
[11] G. Ren, J. Smith, J. Tang, and Y. Xie. "Underground excavation shape optimization using an evolutionary procedure". *Computers and Geotechnics*, vol. 32, n. 2, pp. 122–132, 2005.

[12] G. Ren, Z. Zuo, Y. Xie, and J. Smith. "Underground excavation shape optimization considering material nonlinearities". *Computers and Geotechnics*, vol. 58, pp. 81–87, 2014.
[13] J. Eliáš, L. Mička, and others. "Shape optimization of concrete buried arches". *Engineering Structures*, vol. 48, pp. 716–726, 2013.
[14] M. Sobótka. "Shape optimization of flexible soil-steel culverts taking non-stationary loads into account". In *Structures*, volume 23, pp. 612–620, 2020.
[15] K. F. Seitz and J. Grabe. "Three-dimensional topology optimization for geotechnical foundations in granular soil". *Computers and Geotechnics*, vol. 80, pp. 41–48, 2016.
[16] I. Cavalcante, E. Tavares, R. Picelli, and J. Labaki. "Influence of foundation flexibility on the topology optimization of piled structures (submitted)". *Computers and Geotechnics*, vol. 1, pp. 1–27, 2021.
[17] K. J. Bathe. *Finite Element Procedures*. Prentice Hall, Pearson Education, Inc., 2006.
[18] K. Willner. "Fully coupled frictional contact using elastic halfspace theory". *Journal of Tribology*, vol. 130, 2008.
[19] J. Boussinesq. *Application dès potentiels a l'étude de l'équilibre et du mouvement des solides élastiques*. Gauthier-Villars, 1885.
[20] J. R. Dydo and H. R. Busby. "Elasticity solutions for constant and linearly varying loads applied to a rectangular surface patch on the elastic half-space". *Journal of Elasticity*, vol. 38, n. 2, pp. 153–163, 1995.
[21] D. Carneiro, P. Barros, and J. Labaki. "Ground vibration attenuation performance of surface walls (submitted)". *Journal of Vibration and Control*, vol. 1, pp. 1–38, 2021.